Plant Biotechnology Journal
Open Access

Plant Biotechnology Journal (2022) **20**, pp. 89–102 doi: 10.1111/pbi.13697

CRISPR/*Sp*Cas9-mediated double knockout of barley Microrchidia MORC1 and MORC6a reveals their strong involvement in plant immunity, transcriptional gene silencing and plant growth

Matteo Galli[1], Engie Martiny[1], Jafargholi Imani[1], Neelendra Kumar[1], Aline Koch[2], Jens Steinbrenner[1] and Karl-Heinz Kogel[1,*]

[1]*Institute of Phytopathology, Research Centre for BioSystems, Land Use and Nutrition, Justus Liebig University Giessen, Giessen, Germany*
[2]*Institute for Phytomedicine, University of Hohenheim, Stuttgart, Germany*

Received 1 July 2021;
revised 4 August 2021;
accepted 5 August 2021.
**Correspondence* (Tel +49 641/99-37492; fax +49 641/99-37499; email karl-heinz.kogel@agrar.uni-giessen.de)

Keywords: Microrchidia, barley, *Blumeria graminis*, disease resistance, *Fusarium graminearum*, gene editing, RNA interference.

Summary

The Microrchidia (MORC) family proteins are important nuclear regulators in both animals and plants with critical roles in epigenetic gene silencing and genome stabilization. In the crop plant barley (*Hordeum vulgare*), seven *MORC* gene family members have been described. While barley *HvMORC1* has been functionally characterized, very little information is available about other *HvMORC* paralogs. In this study, we elucidate the role of *HvMORC6a* and its potential interactors in regulating plant immunity via analysis of CRISPR/*Sp*Cas9-mediated single and double knockout (dKO) mutants, *hvmorc1* (previously generated and characterized by our group), *hvmorc6a,* and *hvmorc1/6a*. For generation of *hvmorc1/6a*, we utilized two different strategies: (i) successive *Agrobacterium*-mediated transformation of homozygous single mutants, *hvmorc1* and *hvmorc6a,* with the respective second construct, and (ii) simultaneous transformation with both *hvmorc1* and *hvmorc6a* CRISPR/*Sp*Cas9 constructs. Total mutation efficiency in transformed homozygous single mutants ranged from 80 to 90%, while upon simultaneous transformation, *Sp*Cas9-induced mutation in both *HvMORC1* and *HvMORC6a* genes was observed in 58% of T0 plants. Subsequent infection assays showed that *Hv*MORC6a covers a key role in resistance to biotrophic (*Blumeria graminis*) and necrotrophic (*Fusarium graminearum*) plant pathogenic fungi, where the dKO *hvmorc1/6a* showed the strongest resistant phenotype. Consistent with this, the dKO showed highest levels of basal *PR* gene expression and derepression of *TEs*. Finally, we demonstrate that *Hv*MORC1 and *Hv*MORC6a form distinct nucleocytoplasmic homo-/heteromers with other *Hv*MORCs and interact with components of the RNA-directed DNA methylation (RdDM) pathway, further substantiating that MORC proteins are involved in the regulation of TEs in barley.

Introduction

Microrchidia (MORC) proteins have been identified in many prokaryotes and eukaryotes to facilitate DNA structure rearrangement and DNA mismatch repair (Iyer *et al*., 2008). In plants, like in mammals, MORCs are involved in transcriptional gene silencing and maintenance of genome stability (Kang *et al*., 2008, 2010; 2012; Lorković *et al*., 2012; Moissiard *et al*., 2012, 2014; Brabbs *et al*., 2013; Langen *et al*., 2014; Harris *et al*., 2016; Koch *et al*., 2017; Kumar *et al*., 2018; Xue *et al*., 2021). In Arabidopsis, MORC1 was discovered in a forward genetic screen against turnip crinkle virus (TCV), suggesting that MORCs also play a role in plant immunity (Kang *et al*., 2008). Subsequent genome-wide analyses have detected seven *MORC* genes (*AtMORC1-7*) and many orthologs in various monocotyledon and dicotyledon plants (Dong *et al*., 2018; Langen *et al*., 2014). Plant MORC protein architecture is conserved between species, usually consisting of a GHKL (Gyrase, Hsp90, Histidine Kinase, MutL) domain and an ATPase domain at the N-terminus of the protein, followed by an S5-fold domain and a coiled-coil (CC) or zinc-finger CW (named for its conserved cysteine and tryptophan residues) domain at the C-terminus (Iyer *et al*., 2008; Koch *et al*., 2017). *At*MORC proteins, especially *At*MORC1, *At*MORC2, and *At*MORC6 are involved in multiple layers of defence response against a variety of pathogens, such as TCV, the bacterium *Pseudomonas syringae*, and the oomycete *Hyaloperonospora arabidopsidis* by acting as positive modulators of immunity (Bordiya *et al*., 2016; Harris *et al*., 2016; Kang *et al*., 2008, 2012). Furthermore, in response to microbial pathogens or their microbe-associated patterns (MAMPs), *At*MORC1 was shown to translocate to the plant cell nucleus, where it plays a role in DNA recombination and DNA repair (Kang *et al*., 2008, 2010 and 2012). MORCs' action in the nucleus has been linked to the RNA-directed DNA methylation (RdDM) pathway, which is involved in transcriptional gene silencing (TGS) and chromatin remodelling (Lorković *et al*., 2012; Manohar *et al*., 2017; Moissiard *et al*., 2012; Xue *et al*., 2021). MORCs have also been studied in barley (*Hordeum vulgare,* viz., *Hv*MORC1 and *Hv*MORC2), potato (*Solanum*

© 2021 The Authors. *Plant Biotechnology Journal* published by Society for Experimental Biology and The Association of Applied Biologists and John Wiley & Sons Ltd. This is an open access article under the terms of the Creative Commons Attribution-NonCommercial-NoDerivs License, which permits use and distribution in any medium, provided the original work is properly cited, the use is non-commercial and no modifications or adaptations are made.

tuberosum viz. *St*MORC1), tomato (*Solanum lycopersicum*, viz., *Sl*MORC1), and tobacco (*Nicotiana benthamiana,* viz., *Nb*MORC1) and surprisingly, the role of each MORC protein in plant defence is species-specific (Kumar *et al*., 2018; Langen *et al*., 2014; Manosalva *et al*., 2015). While in Arabidopsis and potato MORC proteins are positive regulators in pathogen resistance, in barley, tobacco, and tomato, they negatively affect plant immunity (Kang et al., 2008, 2010, 2012; Kumar *et al*., 2018; Langen *et al*., 2014; Manosalva *et al*., 2015).

As in Arabidopsis, seven members of the MORC family have been identified in barley, with five closely related to *At*MORC proteins and two to human *Hs*MORC1 to *Hs*MORC4. The Arabidopsis-like group comprises of *Hv*MORC1 [HORVU7Hr1G083280.15], *Hv*MORC2 [HORVU1Hr1G006770.1], *Hv*MORC6a [HORVU3Hr1G046280.3], *Hv*MORC6b [HORVU3Hr1G078330.4], and *Hv*MORC7 [HORVU2Hr1G066650.2], while *Hv*MORCCW1 [HORVU1Hr1G080470.1] and *Hv*MORCCW2 [HORVU7Hr1G093640.4], carrying a CW domain at the C-terminal region of the protein instead of the typical CC, belongs to the human-like clade (Koch *et al*., 2017). In marked contrast to corresponding Arabidopsis mutants, barley *hvmorc1* and *hvmorc2* mutants were more resistant to the biotrophic pathogen *Blumeria graminis* f.sp. *hordei* (*Bgh*) and the necrotrophic pathogen *Fusarium graminearum* (*Fg*) (Kumar *et al*., 2018; Langen *et al*., 2014). On the other hand, like *atmorc1* mutants, barley *hvmorc1* mutants showed derepression of transposable elements (TEs), further suggesting their engagement in genome stabilization (Kumar *et al*., 2018).

Here, we used the CRISPR-Cas9 systems from *Streptococcus pyogenes* (CRISPR/*Sp*Cas9) to generate *hvmorc6a* KO mutants and *hvmorc1*/*hvmorc6a* dKO mutants to further explore the role of *Hv*MORC1 and *Hv*MORC6a in plant immunity. *Hv*MORC6a shares 58.2% aa similarity with *At*MORC6 and 55.0% with *At*MORC1. *At*MORC6 was reported to function in the condensation of pericentromeric heterochromatin, thereby facilitating transcriptional silencing. Furthermore, it has been hypothesized that *At*MORC1 and *At*MORC2 form small nuclear heterodimers with *At*MORC6, which then act in the nucleus and are required for Pol V occupancy in the RdDM pathway (Liu *et al*., 2016; Moissiard *et al*., 2014). Here, we demonstrate that *Hv*MORC6a, like *Hv*MORC1, is involved in disease resistance against biotrophic and necrotrophic pathogens. We show that *Hv*MORC1 and *Hv*MORC6a form nucleocytoplasmic homo-/heteromers, interact with components of the epigenetic gene silencing machinery, and function as repressors of transposable elements (TE).

Results

CRISPR/*Sp*Cas9-mediated generation of KO *hvmorc6a* and dKO *hvmorc1/6a* mutants

In barley, *Hv*MORC1 has been shown to increase disease resistance to fungal pathogens and to derepress the expression of transposable elements (TEs) (Kumar *et al*., 2018; Langen *et al*., 2014). On the other hand, the role of *Hv*MORC6a in modulating plant immunity and genome stabilization is inadequately understood. To assess the function of the *Hv*MORC6a protein, we generated *hvmorc6a* and *hvmorc1/6a* mutants using CRISPR/*Sp*Cas9. Towards this, we generated *hvmorc6a*-guided RNA, with no potential off-target sites (see Experimental Procedures) in the barley genome or other barley MORC family genes (*HvMORC1, HvMORC2*, *HvMORC6b*, *HvMORC7*, *HvMORCCW1,* and *HvMORCCW2*). To completely disable the *Hv*MORC6a function, sgRNA targeted the 5′ part of *HvMORC6a*, upstream the ATPase domain, and generated plants with *HvMORC6a* loss-of-function alleles (Figure S1a–d). After *Agrobacterium*-mediated transformation and germination of the transformed seedlings, genome editing activity was investigated in 2-week-old first generation (T0) plants. The genomic target region was amplified by PCR and the amplicons were analysed by Sanger sequencing using specific primers (Table S1). Out of 123 candidate *hvmorc6a* plants, 93 plantlets carried Indel mutations within the 20 bp target sequence (76% mutation efficiency), of which 42 contained a bi-allelic homozygous mutation (identical mutation on both alleles) (Figure S2a). *Sp*Cas9 also induced different mutation patterns in T0 plants, including bi-allelic heterozygous mutations (different mutations on the two alleles) (Figure S2b,c). This phenotype was confirmed by the characteristic presence of double peaks in the sequencing chromatogram (Figure S2d).

Next, using *Sp*Cas9, we generated dKO barley plants, mutated in both *HvMORC1* and *HvMORC6a*. To ensure the correct generation of the desired dKO genotype, we utilized two different strategies: (i) simultaneous transformation of wild-type (WT) barley cv. Golden Promise with both *hvmorc1* (Kumar *et al*., 2018) and *hvmorc6a* CRISPR/*Sp*Cas9 constructs, and (ii) transformation of homozygous single mutants with the second construct, where *hvmorc6a* plants were transformed with the *hvmorc1* construct and *hvmorc1* plants were transformed with the *hvmorc6a* construct. For the latter (ii), only single mutants devoid of the T-DNA construct, in which the *hygromycin B* gene could not be detected anymore, were used for transformation. Using both strategies, 55 *morc1* in *morc6a*, 64 *morc6a* in *morc1* and 147 *morc1/6a* T0 266 plants were generated, and *Sp*Cas9-induced mutation efficiencies were compared (Figure 1a). Total mutation efficiency in transformed homozygous single mutants was 89% and 81% with respective *hvmorc1*- and *hvmorc6a*-guided RNA. In the simultaneous transformation, *Sp*Cas9-induced mutations of both *HvMORC1* and *HvMORC6a* genes were observed in 58% of the analysed plants. Thus, we already found in T0 generation plantlets that carried disrupted bi-allelic homozygous mutations in both target genes (17 of 64 in *hvmorc6a* transformed plants, 27%; 13 of 55 plants in *hvmorc1*, 23%; 12 of 147 plants in the simultaneous transformation, 8%).

CRISPR/*Sp*Cas9-generated *hvmorc6a* and *hvmorc1/6a* mutants display no off-target effects in other barley *MORC*s

Homozygous bi-allelic genome-edited T0 *hvmorc6a* and *hvmorc1/6a* plants were selected and propagated in soil to obtain T1 seeds. We further worked only with T1 lines that carried a disruptive mutation in target gene(s): Δ*hvmorc6a*-L9 and L16 carrying a 1bp insertion and 25bp deletion respectively in *HvMORC6a*; and Δ*hvmorc1/6a*-L4 and L5 harbouring both a 2bp deletion in *HvMORC1* and 1 bp insertion and 8 bp deletion respectively in *HvMORC6a* (Figure S3a). First, expression of *HvMORC* homologs was assessed in mutants to confirm the KO phenotype and study possible off-target effects. To this end, *HvMORC1*, *HvMORC2*, *HvMORC6a*, *HvMORC7,* and *HvMORCCW1* transcripts were determined by RT-qPCR in 3-week-old WT, *hvmorc1*, *hvmorc6a*, and *hvmorc1*/6a mutant plants. Notably, transcript levels of *HvMORC1* and *HvMORC6a* were significantly downregulated (~80% reduction) in corresponding mutants, while those of other *HvMORCs* remained unaltered (Figure 1b). As anticipated, further sequencing analysis confirmed that the reduced transcript level of *HvMORC1* and

(a)

CRISPR/*Sp*Cas9 construct	p*Hv*U3:***morc1***:sgRNA:p*Zm*Ubi:*Sp*Cas9 in *hvmorc6a*	p*Hv*U3:***morc6a***:sgRNA:p*Zm*Ubi:*Sp*Cas9 in *hvmorc1*	p*Hv*U3:***morc1***:sgRNA:p*Zm*Ubi:*Sp*Cas9 + p*Hv*U3:***morc6a***:sgRNA:p*Zm*Ubi:*Sp*Cas9 in barley wildtype
Nr. of plants	55	64	147
Mutation frequency in T0 plants	50 (89%)	52 (81%)	85 (58%)
Bi-allelic homozygous dKO	13 (23%)	17 (27%)	12 (8%)
Pattern of mutation detected	1bp+, 1bp-, 2bp- and 5bp-	1bp+, 2bp-, 5bp-, 9bp- and 25bp-	1bp+, 1bp-, 2bp- and 25bp-

Barley CRISPR/*Sp*Cas9 *Agrobacterium*-mediated transformation

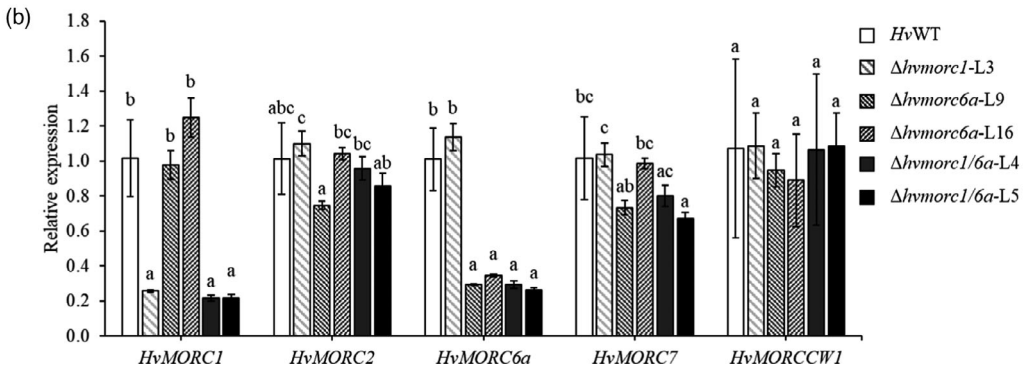

Figure 1 Mutation efficiency and silencing effect in *Sp*Cas9-induced *hvmorc1/6a* dKO mutants. (a) Schematic summary of CRISPR efficacy in the generation of *hvmorc1/6a* dKO in different backgrounds. For transformation with second construct, *hvmorc1* and *hvmorc6a* T2 transgene-free plants were used (Δ*hvmorc1*-L3, Δ*hvmorc6a*-L9). For simultaneous transformation, WT barley plants were transformed with both sgRNAs. (b) Relative *MORC* expression in leaves of barley WT, *hvmorc1* (Δ*hvmorc1*-L3), *hvmorc6a* (Δ*hvmorc6a*-L9 and L16) and *hvmorc1/6a* (Δ*hvmorc1/6a*-L4 and L5) T3 mutants. Transcript amounts of *HvMORC1*, *HvMORC2*, *HvMORC6a, HvMORC7,* and *HvMORCCW1* were measured in the second youngest leaf of 21 days old plants ($n = 8$) via RT-qPCR. Plant ubiquitin (*HvUbiquitin*) was used as the normalization gene. The experiment was repeated twice with similar results. Comparisons between groups were performed via ANOVA and Tukey's range test for multiple comparisons. Letters represent statistical differences among all group means ($\alpha < 0.05$).

HvMORC6a is the result of mRNA degradation by the nonsense-mediated mRNA decay pathway which is involved in degradation of aberrant mRNAs harbouring multiple premature STOP codons (Figure S3b; Reviewed in Yi *et al*., 2020).

*Hv*MORC6a has a negative regulatory role on barley immunity against biotrophic and necrotrophic fungi

Previous results suggest that MORC proteins are modulators of immunity in a species-specific manner (for details see Koch *et al*., 2017). To further explore the role of MORC proteins in barley immunity, we assessed the resistance of *hvmorc6a* and *hvmorc1/6a* plants to the biotrophic powdery mildew fungus. Detached leaves of the virulent barley cv. Golden Promise were inoculated with conidia of *Bgh* race A6 and *Bgh* colonies were counted 5 days post-inoculation (dpi). Compared with WT, all mutant lines *hvmorc1* (Δ*hvmorc1*-L3), *hvmorc6a* (Δ*hvmorc1*-L9 and Δ*hvmorc1*-L16), and *hvmorc1/6a* (Δ*hvmorc1/6a*-L4 and Δ*hvmorc1/6a*-L5) showed increased resistance to *Bgh*. These results were consistent with our expectation that barley MORC paralogs respond similarly to *Bgh* (Kumar *et al*., 2018; Langen *et al*., 2014). Of note, compared with WT plants, dKO lines displayed the strongest phenotype (Δ*hvmorc1/6a*-L4: 55% and Δ*hvmorc1/6a*-L5: 50%), while single mutant lines retain a more moderate resistance (Δ*hvmorc1*-L3: 77%, Δ*hvmorc6a*-L9: 79%, Δ*hvmorc6a*-L16: 72%) (Figure 2a).

Defence pathways involved in resistance to biotrophic and necrotrophic pathogens often function antagonistically (Glazebrook, 2005; Jarosch *et al*., 1999; Klessig *et al*., 2018; Pieterse *et al*., 2012). With this in mind, we also investigated the resistance of all mutants against the necrotroph *Fusarium graminearum* (*Fg*). Detached leaves were drop-inoculated with 20 μL of a macroconidia suspension (5×10^4 conidia mL^{-1}) and infection was assessed via qPCR at five dpi. A significant reduction in fungal growth was observed in both *hvmorc6a* and *hvmorc1/6a* mutants as compared with WT (Δ*hvmorc6a*-L9: 84%, Δ*hvmorc6a*-L16: 82%, and Δ*hvmorc1/6a*-L4: 70%; Figure 2b).

Basal expression of *pathogenesis-related* (*PR*) genes is enhanced in *hvmorc* mutants

Arabidopsis mutants defective in RdDM show enhanced bacterial resistance, and constitutive expression of *Pathogenesis-related 1* (*PR1*) (Yu *et al*., 2013). Similarly, depletion of *HvMORC1* in barley resulted in higher expression of canonical markers for disease resistance, such as *PR* genes (Kumar *et al*., 2018). Based on these findings, we investigated whether KO of *HvMORC6a* also influences expression of *PR* genes and jasmonic acid (JA) marker gene *S-adenosyl-l-methionine: jasmonate O-methyltransferase* (*HvJMT*). The basal expression level of *HvPR1b* (GenBank: X74940.1), *HvPR2* (GenBank: AF479647.2), *HvPR5* (GenBank: AM403331.1) as well as *HvJMT* (GenBank: KAE8819745.1) was determined by RT-qPCR in 3-week-old *hvmorc6a* and *hvmorc1*/6a homozygous plants. Compared with WT, *hvmorc6a* and *hvmorc1*/6a displayed higher *PR* expression levels (fold increase,

© 2021 The Authors. *Plant Biotechnology Journal* published by Society for Experimental Biology and The Association of Applied Biologists and John Wiley & Sons Ltd.,

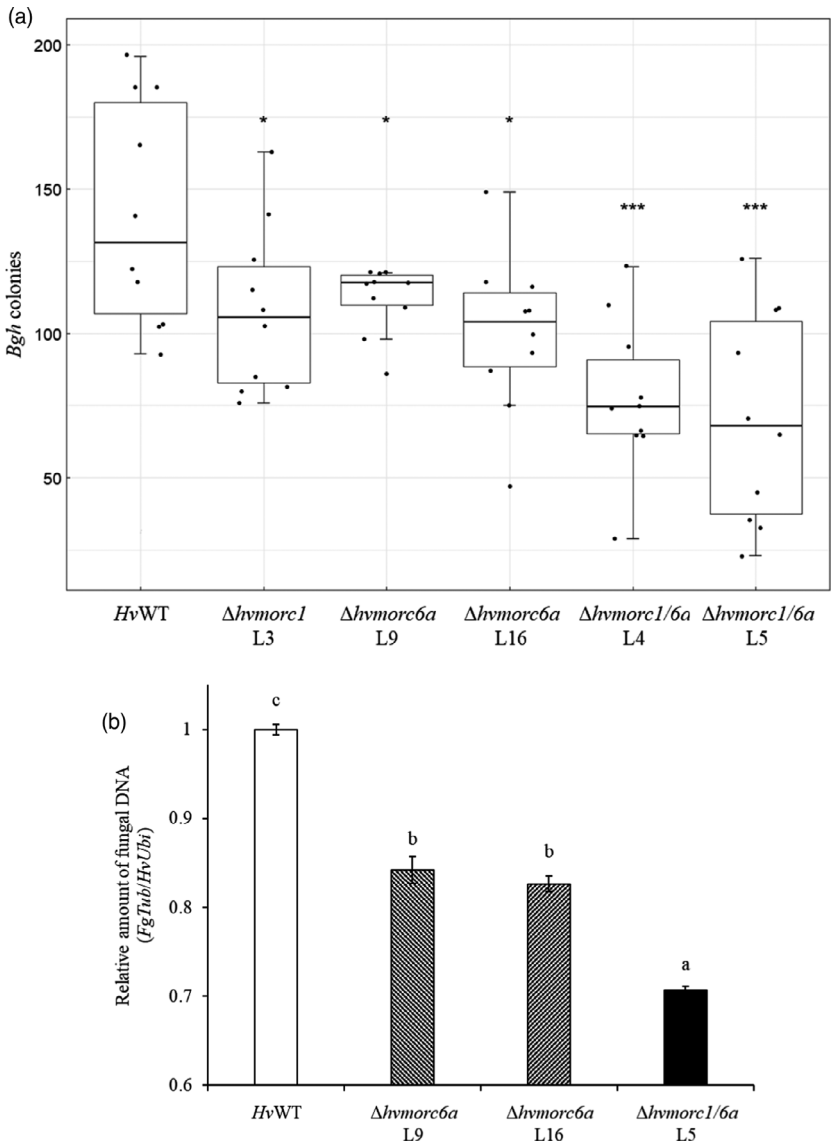

Figure 2 Fitness analysis of *Sp*Cas9-induced mutated lines against fungal pathogens. (a) *hvmorc1* (Δ*hvmorc1*-L3), *hvmorc6a* (Δ*hvmorc6a*-L9 and L16), and *hvmorc1/6a* (Δ*hvmorc1/6a*-L4 and L5) T3 mutants show increased resistance to the biotrophic fungus *Blumeria graminis* f.sp. *hordei* race A6 (*Bgh*). Detached second leaves of 2-week-old plants were inoculated with 3–5 conidia per mm^2 and at 5 dpi, *Bgh* colonies were counted. Shown is the average number of *Bgh* colonies on a 1.5 cm^2 leaf area ($n = 10$). The experiment was repeated twice with similar results. Comparisons between groups were performed via student's t-test between *Hv*WT and mutant lines; asterisks represent statistical difference of the groups against *Hv*WT (*$P < 0.05$; ***$P < 0.001$). (b) *hvmorc6a* (Δ*hvmorc6a*-L9 and L16) and *hvmorc1/6a* (Δ*hvmorc1/6a*-L4 and L5) T3 mutants display enhanced resistance against *Fusarium graminearum* (*Fg*) growth. Detached second leaves of 2-week-old plants were inoculated via drop inoculation assay with 20 µl solution of *Fg* conidia (5×10^4 conidia mL^{-1}). Quantitative PCR was used to measure the *Fg* DNA amount on leaves at 5 dpi (ratio between fungal tubulin to plant ubiquitin; *FgTub/HvUbi*). Bars represent the standard deviation of three technical repetitions; assay was repeated twice with similar results. Comparisons between groups were performed via ANOVA and Tukey's range test for multiple comparisons. Letters represent statistical differences among all group means ($\alpha < 0.05$).

HvPR1b: Δ*hvmorc6a*-L9: 2.1, Δ*hvmorc6a*-L16: 3, Δ*hvmorc1/6a*-L4: 3.6, Δ*hvmorc1/6a*-L5: 4.1; *HvPR2*: Δ*hvmorc6a*-L9: 2.7, Δ*hvmorc6a*-L16: 3, Δ*hvmorc1/6a*-L4: 2.7, Δ*hvmorc1/6a*-L5: 3.9; *HvPR5*: Δ*hvmorc6a*-L9: 2.6, Δ*hvmorc6a*-L16: 2.5, Δ*hvmorc1/6a*-L4: 4.6, Δ*hvmorc1/6a*-L5: 3.4; *HvJMT*: Δ*hvmorc6a*-L9: 2.1, Δ*hvmorc6a*-L16: 1.8, Δ*hvmorc1/6a*-L4: 2.9, Δ*hvmorc1/6a*-L5:3; Figure 3). Most strikingly, expression of all *PR* genes and the *JA* marker gene was strongly induced in the *hvmorc1/6a* mutants.

*Hv*MORC6a is involved in TGS-mediated transposable element silencing

*At*MORC1 and *At*MORC6 have been shown to influence gene silencing downstream of the RdDM pathway, thereby influencing methylation rate and chromatin state (Manohar *et al*., 2017; Moissiard *et al*., 2012). As observed in Arabidopsis *atmorc1* mutant, *hvmorc1* plants showed derepression of TEs, raising the hypothesis that *Hv*MORC1 contributes to genome stabilization (Kumar *et al*., 2018; Langen *et al*., 2014). To prove this further, we assessed the effect of *Hv*MORC6a on TE derepression. Analysing transcription profiles of long terminal repeat (LTR) and non-LTR retrotransposons *HvInga*, *HvRLG-S*, *HvVagabond*, *HvBianca* and *HvCereba* by RT-qPCR, we found increased derepression of TEs in leaves of all *hvmorc* mutants, with significant higher derepression in *hvmorc1/6a* (fold increase, *HvInga*: Δ*hvmorc1*-L3: 1.7, Δ*hvmorc6a*-L9: 2.1, Δ*hvmorc6a*-L16: 2.1, Δ*hvmorc1/6a*-L4: 3.2, Δ*hvmorc1/6a*-L5: 3.5; *HvRLG-S*: Δ*hvmorc1*-L3: 3.7, Δ*hvmorc6a*-L9: 6.4, Δ*hvmorc6a*-L16: 6.5, Δ*hvmorc1/6a*-L4: 10.8, Δ*hvmorc1/6a*-L5: 11.5; *HvVagabond*: Δ*hvmorc1*-L3: 1.5, Δ*hvmorc6a*-L9: 1.6, Δ*hvmorc6a*-L16: 1.3, Δ*hvmorc1/6a*-L4: 21, Δ*hvmorc1/6a*-L5: 18.4; *HvBianca*: Δ*hvmorc1*-L3: 3.6, Δ*hvmorc6a*-L9: 3.8, Δ*hvmorc6a*-L16: 3.2, Δ*hvmorc1/6a*-L4: 6.4, Δ*hvmorc1/6a*-L5: 5.1; *HvCereba*: Δ*hvmorc1*-L3: 1.1, Δ*hvmorc6a*-L9: 1.8, Δ*hvmorc6a*-L16: 2, Δ*hvmorc1/6a*-L4: 3.2, Δ*hvmorc1/6a*-L5: 2; Figure 4).

*Hv*MORC proteins form homomers and heteromers *in vivo*

Because Arabidopsis MORCs form homo-/heteromeric complexes *in vivo* (Harris *et al*., 2016; Liu *et al*., 2014; Moissiard *et al*., 2014), we next performed Y2H assays to determine whether barley MORCs can also interact *in vivo*. We found that *Hv*MORC1 forms both a homomer and heteromers with *Hv*MORC6a, respectively

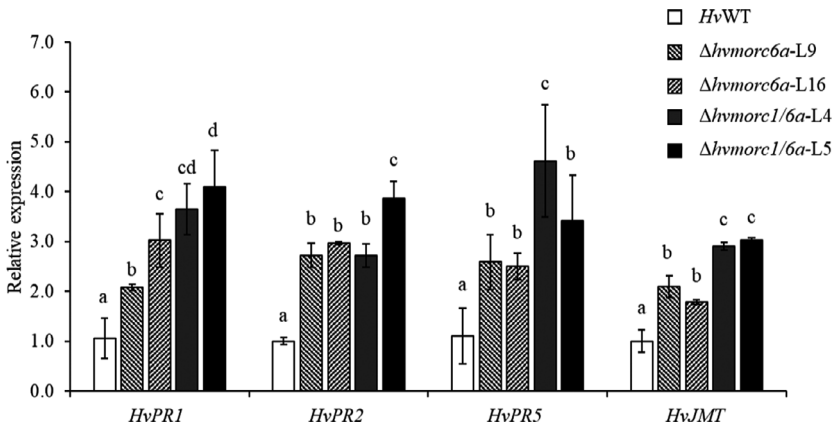

Figure 3 Basal PRs expression in *Sp*Cas9-induced mutated lines. Relative *PR* gene expression in leaves of *Sp*Cas9-generated *hvmorc6a* (Δ*hvmorc6a*-L9 and L16) and *hvmorc1/6a* (Δ*hvmorc1/6a*-L4 and L5) T3 mutants vs. WT. The quantification level of *HvPR1b*, *HvPR2, HvPR5,* and *HvJMT* was measured in the sterile third youngest leaf of 21-day-old plants ($n = 8$) via RT-qPCR. Plant ubiquitin (*HvUbiquitin*) was used as the normalization gene. The experiment was repeated twice with similar results. Comparisons between groups were performed via ANOVA and Tukey's range test for multiple comparisons. Letters represent statistical differences among all group means ($\alpha < 0.05$).

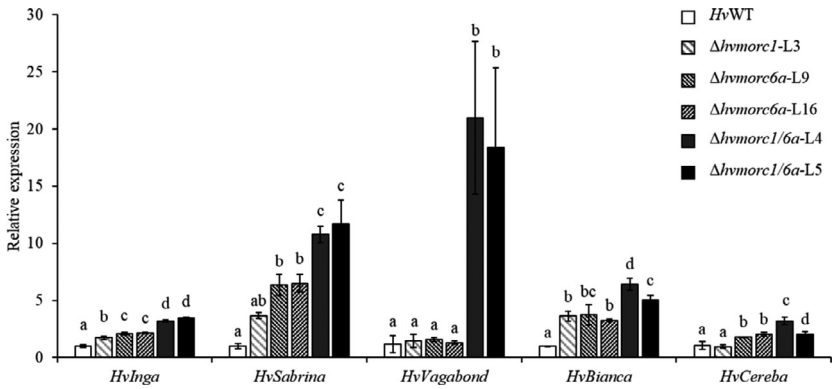

Figure 4 Transposon expression in *Sp*Cas9-induced mutated lines. Relative TEs gene expression in leaves of *Sp*Cas9-generated *hvmorc1* (Δ*hvmorc1*-L3), *hvmorc6a* (Δ*hvmorc6a*-L9 and L16), and *hvmorc1/6a* (Δ*hvmorc1/6a*-L4 and L5) T3 mutants against WT. The quantification level of multiple TEs genes (*HvINGA*, *HvRLG-S*, *HvBianca*, *HvVagabond,* and *HvCereba)* was measured in the second youngest leaf of 21-day-old plants ($n = 8$) via RT-qPCR. Plant ubiquitin (*HvUbiquitin*) was used as the normalization gene. The experiment was repeated twice with similar results. Comparisons between groups were performed via ANOVA and Tukey's range test for multiple comparisons. Letters represent statistical differences among all group means ($\alpha < 0.05$).

(Figure 5a). Moreover, *Hv*MORC2 and *Hv*MORC6a did not form homomeric complexes in our Y2H assays, but *Hv*MORC2 interacted with *Hv*MORC1 and *Hv*MORC6a (Figure 5a).

To further validate our Y2H results *in planta*, a BiFC assay was conducted using *Nicotiana benthamiana* plants. In this approach, the N- and C-terminal parts of YFP were fused to *Hv*MORC1, *Hv*MORC2, and *Hv*MORC6a and were transiently expressed in *N. benthamiana* leaves (Figure 5b, right panel; Figure S4) confirming our Y2H results. Additionally, contrary to the Y2H, we detected a homodimerization for *Hv*MORC2 (Figure 5b, right panel). Surprisingly, and in contrast to *At*MORC6, *Hv*MORC6a did not show any homomeric interaction in either the Y2H assay or the BiFC assay (Figure 5a-b). Furthermore, since it has been hypothesized that *At*MORC1 and *At*MORC2 form small nuclear heterodimers with *At*MORC6, we also transiently expressed chimeric GFP::*Hv*MORC1 and GFP::*Hv*MORC6a under the control of the cauliflower mosaic virus 35S promoter in barley mesophyll protoplasts. Using confocal laser scanning microscopy (CLSM), we examined the precise protein localization in WT and *hvmorc6* barley background (Figure 5b, left panel). For this, barley protoplasts were simultaneously transformed with pSAT6-mCherry-VirD2NLS, serving as a nuclear marker to allow the observation of the nucleus in protoplasts (Citovsky *et al*., 2006; Lin *et al*., 2018). Both *Hv*MORC1 and *Hv*MORC6a showed nucleocytoplasmic localization in the barley WT background (Figure 5b, left panel). Interestingly, in the *hvmorc6a* background, *Hv*MORC1 localized almost exclusively in the cytoplasm while *Hv*MORC6a remained nucleocytoplasmic.

*Hv*MORCs interact with components of the RdDM machinery *in vivo*

*At*MORC1, *At*MORC2, and *At*MORC6 were identified as components of the RdDM pathway by their interaction with SUPPRESSOR OF VARIEGATION 3- 9- (SUV[VAR] 3-9) homologs SUVH2 and/or SUVH9. These two proteins are canonical components of RdDM that interact directly with DEFECTIVE IN MERISTEM

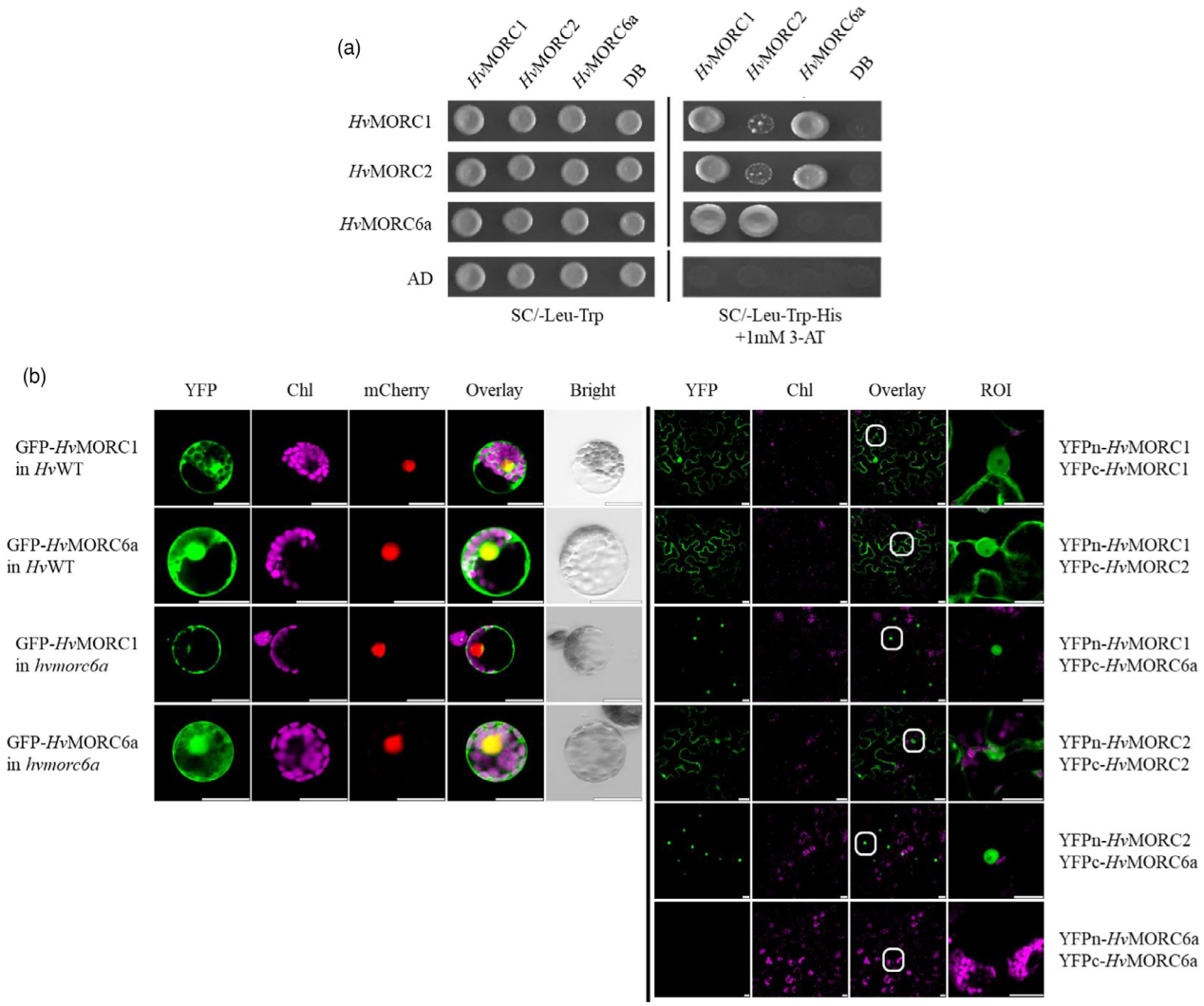

Figure 5 Localization, homomeric and heteromeric interaction of barley MORCs. (a) Y2H screen for possible dimerization between *Hv*MORC proteins. *Hv*MORCs were N-terminally fused to the Gal4-binding domain (DB) and the Gal4 activation domain (AD). Left panel shows growth on SC-Leu–Trp selective media as an indication of successful mating between all combinations. The right panel shows growth on stringent selective media that further lacks histidine and supplemented with 1 mM 3-amino-1,2,4-triazole, a competitive inhibitor of the *HIS3* gene product, indicating interaction between the AD- and DB- constructs and activation of the HIS3 gene. No growth was detected between AD-construct/ DB empty or between DB-construct/AD-empty, indicating that none of the tested constructs is autoactive. (b) GFP signals of barley MORCs detected in barley mesophyll protoplasts after 24 h in barley WT and *hvmorc6a* background (left panel) and YFP signals of homo-/heteromerization of barley MORCs detected in lower epidermal cells of tobacco after 48 h (right panel). p2FGW7-*Hv*MORCs were C-terminally fused to GFP and pBiFP2-*Hv*MORCs and pBiFP3-*Hv*MORCs were C-terminally fused to the N- and C-terminal parts of YFP, respectively. Protoplasts were simultaneously transformed with mCherry-VirD2NLS as a nuclear marker. Images of protoplasts and lower epidermis represent two and three biological replicates, respectively. Scale bar: 20 μm. ROI is a magnification of the bordered region in the overlay column. YFP: yellow fluorescence protein, Chl: chlorophyll autofluorescence, mCherry: nuclear fluorescence, ROI: regions of interest (magnification of the bordered region).

SILENCING 3 (DMS3; Liu *et al*., 2014, 2016; Jing *et al*., 2016). Therefore, we identified orthologs of *At*MORC interactors in barley to further investigate the involvement of *Hv*MORCs in RdDM (Table S2). *Hv*DMS3, *Hv*SUVH9, the double-stranded RNA-binding protein INVOLVED IN DE NOVO 2 (*Hv*IDN2) and the SWITCH SUBUNIT 3C (*Hv*SWI3C) component of the chromatinremodelling complex SWITCH/SUCROSE NON-FERMENTABLE (SWI/SNF) were cloned and tested in a Y2H assay against *Hv*MORC1, *Hv*MORC2, and *Hv*MORC6a. We found that *Hv*MORC1 interacts with *Hv*IDN2 (Figure 6a), in contrast to previous results on *At*MORCs, where Y2H showed no interaction between IDN2 and *At*MORC1 or *At*MORC2 (Liu *et al*., 2016). Consistent with previous Y2H results, revealing an interaction of *At*SUVH9 with *At*MORC1, *At*MORC2, and *At*MORC6 (Liu *et al*., 2014), all three tested *Hv*MORCs interacted with *Hv*SUVH9 (Figure 6a). Surprisingly, none of the tested *Hv*MORCs showed any interaction with *Hv*SWI3C (Figure 6a), which is inconsistent with what was found in *Arabidopsis* (Jing *et al*., 2016). In addition, we did not detect interactions between *Hv*DMS3 with any of the tested *Hv*MORCs (Figure 6a). However, this might be consistent with what was reported for *At*MORCs (Jing *et al*., 2016; Liu *et al*., 2014, 2016; Moissiard *et al*., 2014), since *At*MORC6 interaction with *At*DMS3 was only shown once in an *in vitro* pull-down experiment (Lorković *et al*., 2012) and *in vivo*

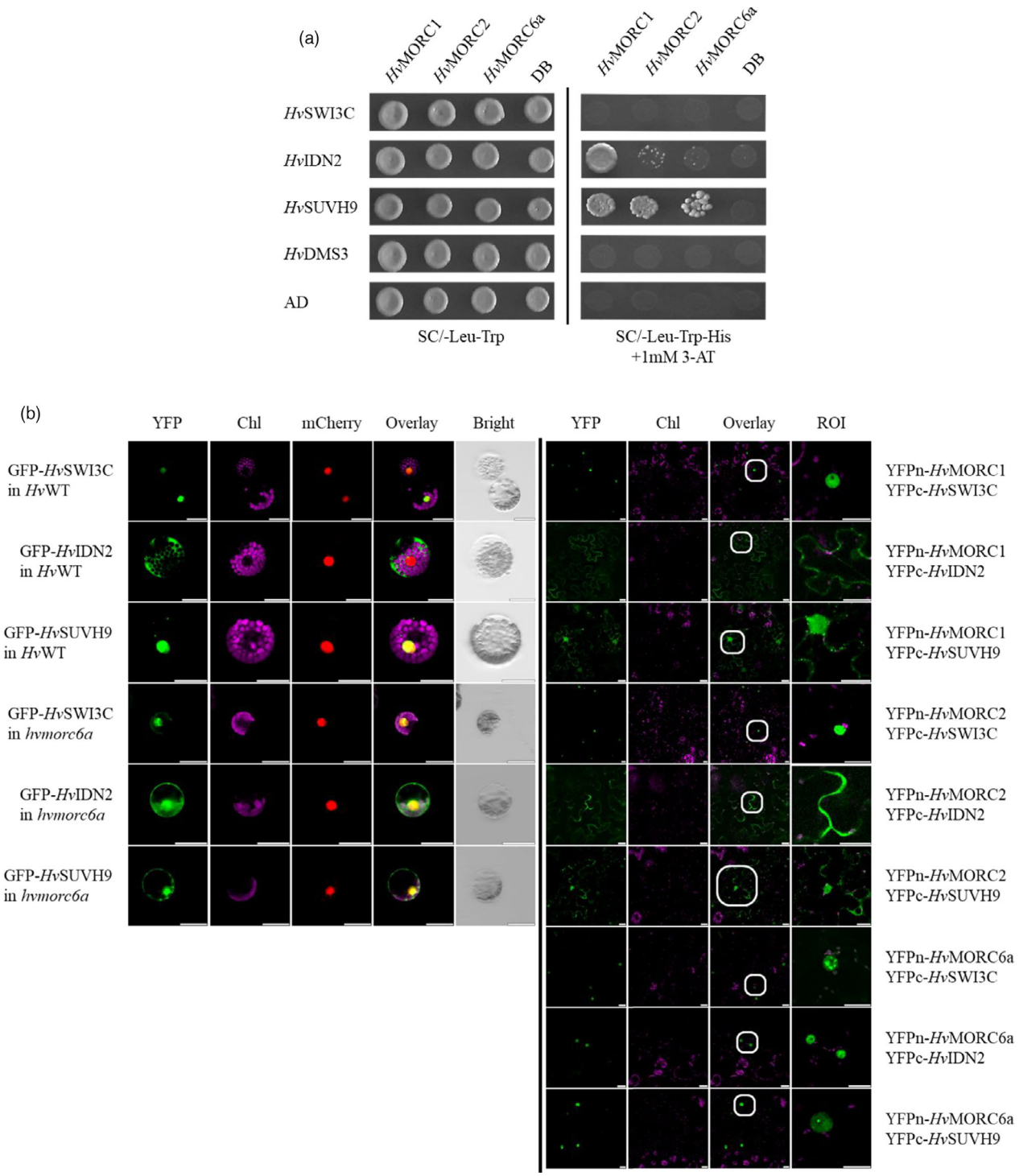

Figure 6 Localization of some barley orthologs of the RdDM pathway and their interactions with barley MORCs. (a) Y2H screen for possible interactions between *Hv*MORCs and *Hv*RdDM components. Barley MORCs and RdDM proteins were N-terminally fused to the Gal4-binding domain (DB) and the Gal4 activation domain (AD). Left panel shows growth on SC-Leu–Trp selective media as an indication of successful mating between all combinations. The right panel shows growth on stringent selective media that further lacks Histidine and supplemented with 1 mM 3-amino-1,2,4-triazole, a competitive inhibitor of the *HIS3* gene product, indicating interaction between the AD- and DB- constructs and activation of the *HIS3* gene. No growth was detected between AD-construct/DB empty or between DB-construct/AD-empty, indicating that none of the tested constructs is autoactive. (b) GFP signals of *Hv*RdDM proteins detected in barley mesophyll protoplasts after 24 h in barley WT and *hvmorc6a* background (left panel) and YFP signals of homo-/heteromerization of barley MORCs detected in lower epidermal cells of tobacco after 48 h (right panel). p2FGW7-*Hv*RdDMs were C-terminally fused to GFP, and pBiFP2-*Hv*MORCs and pBiFP3-*Hv*RdDM were C-terminally fused to the N- and C- terminal parts of YFP, respectively. Protoplasts were transformed with mCherry-VirD2NLS as a nuclear marker. Images of protoplasts and lower epidermis represent two and three biological replicates, respectively. ROI is a magnification of the bordered region in the overlay column. Scale bar: 20 μm. YFP: yellow fluorescence protein, Chl: chlorophyll autofluorescence, mCherry: nuclear fluorescence, ROI: regions of interest (magnification of the bordered region).

© 2021 The Authors. *Plant Biotechnology Journal* published by Society for Experimental Biology and The Association of Applied Biologists and John Wiley & Sons Ltd.,

immunoprecipitation experiments failed to detect the interaction of *At*DMS3 with *At*MORC6, possible due to a weak or ephemeral interaction (Moissiard *et al*., 2014).

Since Y2H only detects approximately 25% of all occurring interactions (Braun *et al*., 2009), we further verified the interactions of *Hv*MORC proteins and the barley RdDM orthologs *in planta* using BiFC in *N. benthamiana* leaf epidermal cells (Figure 6b right panel, Figure S5a–b). BiFC assay revealed an interaction of *Hv*SUVH9 with *Hv*MORC1, *Hv*MORC2, and *Hv*MORC6a, supporting our Y2H results (Figure 6b right panel). Those interactions were predominantly nuclear in epidermal cells of *N. benthamiana* leaves (Figure 6b right panel). Previously, *At*MORC6 was shown to interact with *At*IDN2 (Jing *et al*., 2016). We detected an interaction between *Hv*MORC6a and *Hv*IDN2 in the nucleus of *N. benthamiana* cells (Figure 6b right panel, Figure S5a). The interaction between either *Hv*MORC1 or *Hv*MORC2 with *Hv*IDN2 was entirely cytoplasmic, excluded from the nucleus and was only observed in the nuclear periphery (Figure 6b right panel, Figure S5a). Additionally, we detected interactions between *Hv*MORC1, *Hv*MORC2 or *Hv*MORC6a with *Hv*SWI3C in the nucleus (Figure 6b right panel, Figure S5a), contradictory to our Y2H screens. Finally, and consistent with the Y2H results, we could not detect any interaction of *Hv*MORCs with *Hv*DMS3 *in planta* (Figure S5b). Since *At*MORC6 has been shown to be involved in the regulation of chromatin condensation and we show the interaction in Y2H and BiFC in *N. benthamiana*, we additionally analysed the localization of *Hv*SWI3C, *Hv*IDN2, *Hv*SUVH9, and *Hv*DMS3 in barley WT and *hvmorc6a* background (Figure 6b, left panel; Figure S5b). CLSM of barley WT mesophyll protoplasts revealed that *Hv*SWI3C and *Hv*SUVH9 were exclusively localized to the nucleus, *Hv*IDN2 and *Hv*DMS3 showed a cytoplasmic and nuclear-cytoplasmic localization, respectively (Figure 6b left panel, Figure S5b left panel). In *hvmorc6a* background, *Hv*SWI3C, *Hv*SUVH9, and *Hv*IDN2 could be detected both into the nucleus and in the cytoplasm of the cell (Figure 6b left panel). Lastly, we could not detect any difference in the localization of *Hv*DMS3 (Figure S5b left panel).

*Hv*MORC6a affects plant biomass and growth

High expression of *PR* genes and other defence genes has an impact on plant yield and development (Kumar *et al*., 2021; Xu *et al*., 2017). Based on our findings that *hvmorc* mutants have a high basal level of PRs, we analysed whether KO of *Hv*MORC1 and *Hv*MORC6a affects plant growth and development. For this, we measured the root and shoot biomasses of 3-week-old *hvmorc1*, *hvmorc6a,* and *hvmorc1/6a* plants. While Δ*hvmorc1*-L3 single mutants did show aberrant growth compared with WT (13% reduction of shoots and roots), Δ*hvmorc6a*-L9 and Δ*hvmorc1/6a*-L5 mutants were strongly impaired in growth with root and shoot dry weight lower as compared with WT plants (shoot dry weight 17% and 18% reduction, respectively; root dry weight: 23% and 24% reduction, respectively; Figure 7a–c).

Discussion

Efficient CRISPR/*Sp*Cas9-mediated multiple gene editing in barley

Targeted genome engineering is the modification of the DNA in an organism at a precise, predetermined locus. From an agricultural perspective, gene editing is an important tool to improve yield, grain quality, and resistance/tolerance of crops to biotic and abiotic stress to ensure sustainable, but also effective food production (Fernandez-Cornejo *et al*., 2014; Govindan and Ramalingam, 2016; Kim and Kim, 2014; Zhu *et al*., 2020). Over the last decade, the type II CRISPR-Cas9 editing module has emerged as a powerful tool to induce precise mutations in the genome of many animal and plant species, including barley (Cong *et al*., 2013; Gasparis *et al*., 2018; Holme *et al*., 2017; Jaganathan *et al*., 2018; Kapusi *et al*., 2017; Kis *et al*., 2019; Kumar *et al*., 2018; Lawrenson *et al*., 2015; Lee *et al*., 2021; Li *et al*., 2020; Mali *et al*., 2013; Zeng *et al*., 2020). In a previous study, we already used the barley RNA Polymerase (Pol) III-dependent U3 small nuclear RNA promoter (GenBank: CAJX011995286.1) for efficient sgRNA expression and KO of *HvMORC1* (Kumar *et al*., 2018). Here we show that a *Hv*U3-driven sgRNA construct was equally effective for *HvMORC6a* KO (Figure S1a). After hygromycin selection, using PCR and Sanger sequencing, we detected Indel mutations in 76% of T0 *hvmorc6a* mutants (Figure S2a). The strikingly high mutation frequency supports the technical finding that the *Hv*U3 promoter is suitable to drive sgRNA expression in the type II CRISPR/*Sp*Cas9 system for genome editing in barley. For the generation of the dKO mutant *hvmorc1/6a*, we compared two different strategies: (i) successive *Agrobacterium*-mediated transformation of a homozygous single MORC mutant with the respective second KO construct, and (ii) simultaneous *Agrobacterium*-mediated transformation with two constructs, each targeting one of the two *MORC* genes. Both strategies yielded high mutation rates (Figure 1a). Total mutation efficiency in transformed homozygous single mutants was between 80 to 90%, while in simultaneous transformation, *Sp*Cas9 induced a mutation in both *HvMORC1* and *HvMORC6a* in 58% of T0 generation plants. Expression analyses of *MORC* genes confirmed that the CRISPR/*Sp*Cas9 constructs precisely targeted target *MORC* genes and did not cause off-target effects that resulted in impaired gene activity of other MORC paralogs (Figure 1b). Therefore, our results confirm the effectiveness and usefulness of CRISPR/*Sp*Cas9 genome editing for analysing plant gene function in a multigene family such as that of barley *MORCs*.

*Hv*MORC6a is involved in plant defence and interacts with chromatin remodelling mediator proteins

In mammals, MORC proteins are involved in maintaining genome stability and in consequence, the regulation of cancer and other diseases as well as spermatogenesis (Iyer *et al*., 2008), while in plants, they are involved in maintaining genome stability in addition to their function in immunity to microbial pathogens (Koch *et al*., 2017). MORC proteins in cereals are largely unexplored, because in the past, KO mutants were difficult to produce. Previous studies demonstrated that RNAi-mediated knockdown (KD) of *HvMORC1* and *HvMORC2* rendered barley less susceptible to both biotrophic and necrotrophic fungal pathogen (Langen *et al*., 2014), which was subsequently confirmed with CRISPR/*Sp*Cas9-mediated KO of *HvMORC1* (Kumar *et al*., 2018). These findings agreed with earlier reports showing that the Arabidopsis dKO mutant *atmorc1/2* is compromised in the immune response to inoculation with *Pseudomonas syringae pv. maculicola (Psm)* (Kang *et al*., 2012).

The barley *HvMORC6a* gene shares 58% aa similarity with *AtMORC6* (Koch *et al*., 2017). *At*MORC6 acts as positive regulator of defence against the oomycete pathogen *Hyaloperonospora arabidopsidis* (*Hpa*) (Harris *et al*., 2016). In agreement with an immune function of MORC6, we show here that

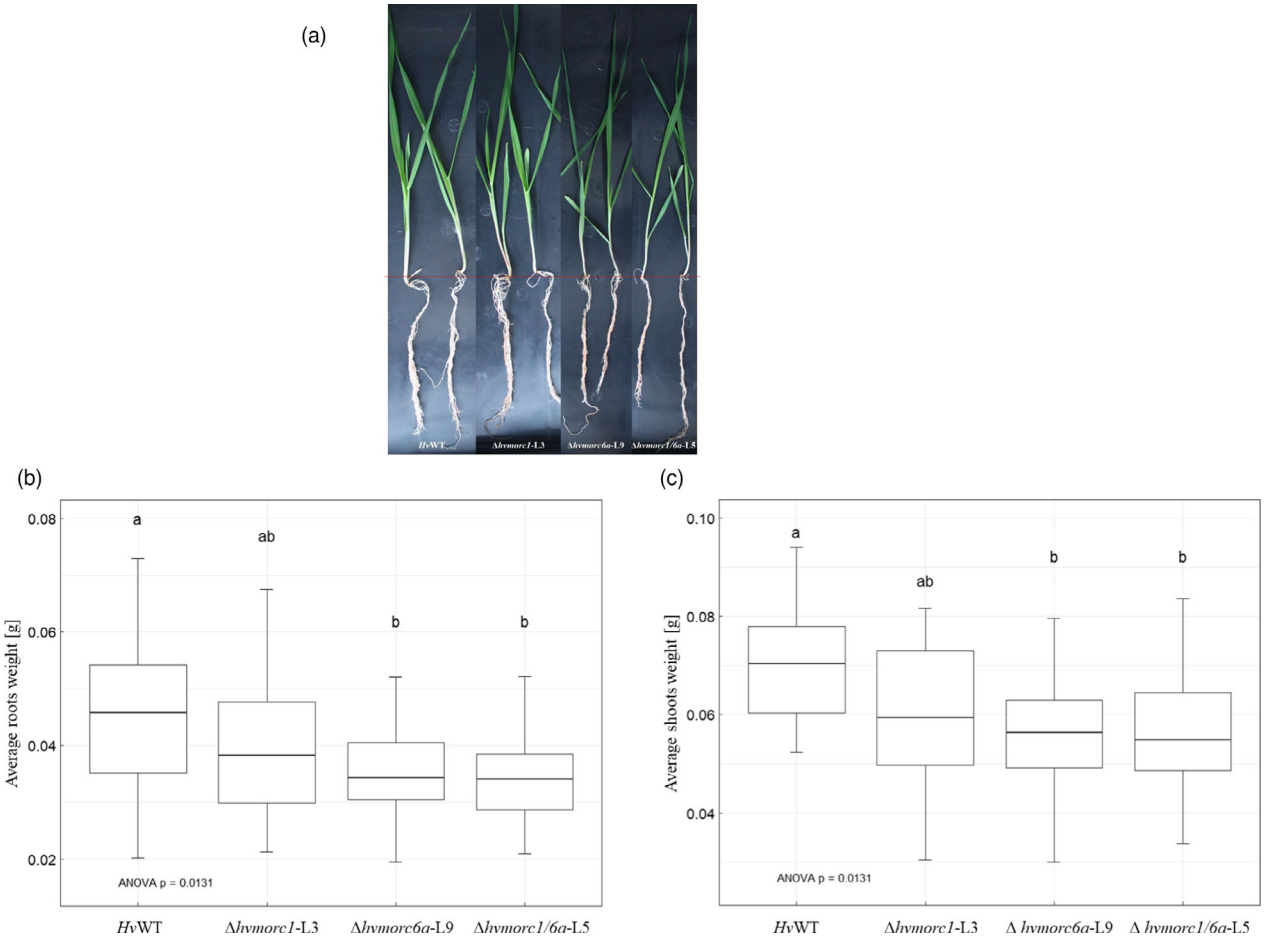

Figure 7 Root and shoot biomass of 3-week-old WT and mutant plants. (a) Plant morphology, (b) roots dry weight, and (c) shoots dry weight of T3 barley plants impaired in the expression of *HvMORC1* (Δ*hvmorc1*-L3), *HvMORC6a* (Δ*hvmorc6a*-L9), and both genes (Δ*hvmorc1/6a*- L5) vs. WT. Plants were cultivated in artificial soil containing a 2:1 mixture of expanded clay (Seramis®, Masterfoods, Verden, Germany) and Oil-Dri® (Damolin, Mettmann, Germany) in a growth chamber at 22 °C/18 °C (day/night cycle) with 60% relative humidity and a photoperiod of 16 h (240 μmol m^{-2} s^{-1} photon flux density). The experiment was conducted two times (n = 15 plants) with similar results. Comparisons between groups were performed via One-way ANOVA and Tukey's Range Test. Letters represent statistical differences among all group means (α = 0.05).

depletion of *HvMORC6a* enhances the resistance of barley against *Bgh* and *Fg* (Figure 2a,b), and is associated with a higher basal expression of *PR* and JA marker genes (Figure 3). Of note, the highly susceptible Arabidopsis dKO mutant *atmorc1/2* showed attenuated expression of *PR* genes upon infection with *P. syringae* pv. *tomato* (*Pst*; Bordiya *et al*., 2016), which confirms the correlation of MORC-mediated immune phenotypes with defence gene expression.

Despite their contrasting effects on plant immunity, both barley and Arabidopsis MORCs control TE expression in a similar manner (Figure 4; Bordiya *et al*., 2016; Langen *et al*., 2014). We do not yet have a profound explanation for this phenomenon. Bordiya and co-workers suggested that *Pst* infection primarily suppresses binding of *At*MORC1 to DNase I hypersensitive sites (dDHSs), regions of the genome where the chromatin has lost its condensed structure, which are associated with heterochromatic TEs, but enhances its binding at infection-induced dDHSs in genes and TEs. Combined with earlier reports, showing the involvement of *At*MORC1 and *At*MORC6 in upregulation of DNA methylation as well as condensation of compact chromatin (Brabbs *et al*., 2013; Lorković *et al*., 2012; Moissiard *et al*., 2012), the data suggest that *At*MORC1 and/or *At*MORC6 are involved in both gene silencing and gene induction. It is likely that in barley, interaction of *Hv*MORC1 and *Hv*MORC6a with DNA modulating proteins near *PR* loci leads to suppression of *PR* transcription, explaining why barley *MORC* mutants show increased *PR* expression and disease resistance to fungal pathogens.

The dKO mutant *hvmorc1/6a* displays the strongest effect on pathogen defence (Figure 2a, b) and *PR* gene (Figure 3) expression in barley. Therefore, data hint at the possibility that *HvMORC1* and *HvMORC6a* interact with each other and suppress plant defence through epigenetic silencing mechanisms. Microscopic localization showed that *Hv*MORC1 in *hvmorc6a* barley protoplasts was predominantly localized in the cytoplasm of the cell compared with the nuclear-cytoplasmatic localization in barley WT (Figure 5b, left panel). This is consistent with the results in Arabidopsis, where MORC1 and MORC2 form homomers and in addition, heteromers with MORC6 (Liu *et al*., 2014; Moissiard *et al*., 2014). Using Y2H and BiFC assays, we could detect heteromerization of *Hv*MORC6a with *Hv*MORC1 and with

© 2021 The Authors. *Plant Biotechnology Journal* published by Society for Experimental Biology and The Association of Applied Biologists and John Wiley & Sons Ltd.,

*Hv*MORC2; and we confirmed complex formation of *Hv*MORC1 with *Hv*MORC2 as found in Arabidopsis. Unlike in Arabidopsis, we could not find homomerization of *Hv*MORC6a, though we could confirm homomerization of *Hv*MORC1 and heteromerization of *Hv*MORC1 with *Hv*MORC2. *Hv*MORC1and *Hv*MORC2 form homomers and heteromers in the cytoplasm and to a lower extent in the nucleus of *N. benthamiana* cells (Figure 5b right panel, Figure S4). In contrast, the interaction of *Hv*MORC1/6a and *Hv*MORC2/6a was mainly found in the nucleus of *N. benthamiana* plants (Figure 5b right panel, Figure S4). *At*MORC1 was shown to interact with several Resistance (R) proteins, preferable in their inactive state, residing at the plasma membrane (Kang *et al*., 2010). Therefore, it seems plausible that *Hv*MORC1 and its homolog *Hv*MORC2 also reside in the cytoplasm of barley cells. On the other hand, our data suggest that *Hv*MORC1 and *Hv*MORC6a heteromerization likely affects heterochromatin condensation, as reflected by the increased TEs and *PRs* expression and disease resistance in the barley dKO mutants.

To further investigate whether suppression of barley TEs is mediated by *Hv*MORC proteins, we tested the interactions of barley MORC family members with selected barley orthologs of the RdDM pathway. In Arabidopsis, *At*SUVH9 together with *At*MORC6 and *At*SUVH2 regulates silencing of some TEs (Liu *et al*., 2016). In addition, the SWI/SNF chromatin remodelling complex components SWI3B, SWI3C, and SWI3D, together with IDN2, interact with *At*MORC6 to mediate TGS at some *At*MORC6-specific loci (Liu *et al*., 2016). It was suggested that *At*MORC proteins act as adaptors to recruit RNA Polymerase V, in conjunction with *At*SUVH2 and *At*SUVH9 to facilitate the production of long non-coding RNAs (lncRNAs) to promote DNA methylation (Jing *et al*., 2016; Liu *et al*., 2014, 2016). Furthermore, it was proposed that *At*MORC1, *At*MORC2 and/or *At*MORC6 act together with the SWI/SNF chromatin remodelling complex components and IDN2 to alter chromatin structure and therefore reinforce TGS (Jing *et al*., 2016; Koch *et al*., 2017; Liu *et al*., 2016). We observed an interaction of the *Hv*MORC1, *Hv*MORC2, and *Hv*MORC6a with *Hv*IDN2, *Hv*SUVH9, and *Hv*SWI3C with nuclear and cytoplasmatic localization in leaf epidermal cells of *N. benthamiana*, and additionally a shift of localization of these RdDM components in cellular compartments between *hvmorc6a* and barley WT protoplasts (Figure 6b, Figure S5a), further indicating that the barley MORC family members are also involved in RdDM-mediated TEs repression in barley through a *Hv*MORC-dependent pathway.

Derepression of MORC-related genes is linked with lower plant biomass and growth

The barley genome, like most of the plant genomes, consists of a big part of transposable elements or transposons (84%) (International Barley Genome Sequencing Consortium, 2012). Even though these elements are categorized in two classes (retroelement and DNA element transposons, members of the first-class transpose through an RNA intermediate while members of the latter one through a DNA intermediate) their function is nonetheless similar: they move through the genomes to activate and deactivate genes, influence their expression and are fundamental in epigenetic regulation (Bennetzen and Wang, 2014; Galindo-González *et al*., 2017). Notably in plants, TE activity was also detected in response to exogenous environmental and genomic stresses (Alzohairy *et al*., 2012; Galindo-González *et al*., 2017; Grandbastien *et al*., 2005; Salazar *et al*., 2007). Stress has normally a direct effect on the activation of the immune system, which comes always at a great cost for plant development and growth (Huot *et al*., 2014; Kumar *et al*., 2021; Xu *et al*., 2017). To assess whether TEs derepression influences plant fitness and development, we measured the root and shoot biomasses of WT and barley MORC mutants, over a growth period of 3 weeks. Both root and shoot dry weight of all the mutants were lower as compared with WT plants (Figure 7b–c), suggesting a positive correlation between transcript levels and growth promotion. Notably, in *hvmorc6a* and *hvmorc1/6a* mutants, we found strong impairment in growth (Figure 7a) indicating probably a major role of *Hv*MORC6a in nuclear stabilization. Our results underline how important it is to keep the natural chromatin compaction and relaxation for proper plant development and growth.

Our work shows a successful example of how genome editing technologies can be used to introduce desirable agronomic traits into a cereal plant. With CRISPR/Cas, we were able to make plants more resistant to biotic stress, and with significantly fewer undesirable side effects on the plant genome than with chemical and radiation mutagenesis. While conventional breeding produces thousands of random mutations and then requires time-consuming backcrossing to isolate a desired new trait, molecular breeding methods, on the other hand, are easy to use, fast, precise, flexible, and cost-effective. For us, there is no evidence-based doubt that this technology will be a fundamental part of every plant breeder's toolbox in the future.

Experimental procedures

Plant material and fungal inoculation

Seeds of spring barley (*Hordeum vulgare*) cv. 'Golden Promise' were germinated on wet filter paper in large plastic Petri plates. Three days after germination, seedlings were transferred to soil and grown in Typ T soil (Fruhstorfer Erde, Vechta, Germany; 200 g capacity pots) under control condition of 16 h light (240 μmol m^{-2} s^{-1} photon flux density) and 60% relative humidity (22/18 °C day/night cycle). For pathogen assays, the second youngest leaves of 14-day-old plants were cut and laid on 0.7% (w/v) water agar and inoculated with powdery mildew fungus race A6 (*Blumeria graminis* f.sp. *hordei*) at a conidia density of 5 per mm^2 by air current dispersion in an inoculation tower and saved in the same climate chamber for 7 days (Langen *et al*., 2014). *Bgh* colonies were counted using a binocular on a 2.5 cm^2 segment. For *Fusarium graminearum*, strain 1003 (Jansen *et al*., 2005) was selected for inoculation, the fungus was cultured on synthetic nutrient-poor agar medium (SNA) at room temperature under constant illumination as described by Kumar *et al*., 2018. Conidia was isolated from 2-week-old plates, by scrubbing using a Drigalski spatula and filtered through a piece of Miracloth (Calbiochem, http://www.merck-chemicals.de). Conidia was finally resuspended in sterile 0.02% Tween water (w/v) and its concentration was adjusted to 5×10^4 spore mL^{-1}. 20 μL of the suspension was drop-inoculated on detached barley leaves. Progression of infection was routinely monitored and quantification of fungal growth was assessed after 5 days post-inoculation (dpi). Leaf samples were crushed and DNA was extracted via DNA extraction kit (Qiagen, Hilden, Germany). The total fungal/plant DNA ratio was quantified via qPCR normalized with fungal tubulin (*FgTub*) to plant ubiquitin (*HvUbi*), respectively (Table S1).

Generation of CRISPR/*Sp*Cas9 constructs and plant transformation

Twenty nucleotides (nt) target sequence present immediately adjacent to a Protospacer Adjacent Motif (PAM) was selected using CRISPR sgRNA design online tool (https://atum.bio/eCommerce/cas9/input) for *HvMORC6a* (GenBank: HORVU3Hr1G046280.3). The designed 20 nt target sequence was blasted (BlastN) against nucleotide collection of *Hordeum vulgare* (taxid: 4513) at NCBI to check for putative off-targets, GTACGGCTTGACATCGCGGGGGG was selected, and sgRNA was assembled and cloned into CRISPR/*Sp*Cas binary destination vector, as described (Kumar *et al*., 2018). The CRISPR/*Sp*Cas9 vector containing *hvmorc6a*-guided RNA was electroporated (Gene Pulser, Bio-Rad) into *Agrobacterium tumefaciens* strain AGL1 (Lazo *et al*., 1991), and the resulting strain was used to transform spring barley 'Golden Promise' as described (Imani *et al*., 2011). For generation of the double KO line (*hvmorc1/6a*), co-knockout of the *hvmorc6a* and *hvmorc1* genes was obtained using a mixture of two *Agrobacterium* cultures which contained *hvmorc6a*- and *hvmorc1*-guided RNA. The *Agrobacterium* pool was cultured with barley immature embryos as described (Imani *et al*., 2011). All putative single and double knockout barley lines were characterized using PCR followed by Sanger sequencing of the genomic region targeted by respective CRISPR sgRNAs.

DNA isolation and quantitative RT-PCR analysis

DNA/RNA extraction and quantitative RT-qPCR were performed as described in protocol kits (DNA: Qiagen, Hilden, Germany; RNA: Zymo Research, Irvine). Primer pairs used for PCR and expression analysis are listed in Table S1.

Gateway cloning and plasmid DNA preparation

To create Gateway entry, clones of coding sequences (CDS) of barley MORCs (clones obtained from previous work; Langen *et al*., 2014) and the candidate interactors from the barley cultivar Golden Promise were amplified from cDNA using *att*B flanked primer pairs (Table S1) and recombined by Gateway cloning into pDONR™/Zeo vector (Invitrogen, UK) according to the manufacturer's recommendations.

For the yeast two-hybrid (Y2H) assay, entry clones were recombined into pAD and pDB destination vectors (N-terminal fusions of Activation domain AD and DNA-Binding domain DB of the *Saccharomyces cerevisiae* transcriptional activator Gal4, respectively) (Dreze *et al*., 2010). For bimolecular fluorescent complementation (BiFC) assay in *N. benthamiana* plants, entry clones were recombined into pBIFP2 and pBIFP3 destination vectors (N-terminal fusions of the N- and C- parts of yellow fluorescence protein YFP, respectively) (Azimzadeh *et al*., 2008). For CLSM assay in barley protoplasts, entry clones were recombined into p2FGW7 destination vector (Karimi *et al*., 2002). Sanger sequencing was used to validate in-frame cloning and the sequence integrity of all constructs using appropriate primers (Table S1).

Yeast transformation and Y2H assay

Two haploid strains of *S. cerevisiae* of opposite mating types Y8800 (MATa) and Y8930 (MATα), with genotype: *leu2-3,112 trp1-901 his3-200 ura3-52 gal4*Δ *gal80*Δ *GAL2-ADE2 LYS2::GAL1-HIS3 MET2::GAL7-lacZ cyh2*^{R} (Dreze *et al*., 2010) were transformed with CDS-containing pAD and pDB (AD-X and DB-Y) plasmids. Yeast transformation was done using the PEG/Lithium acetate heat-shock method, as previously described (Dreze *et al*., 2010). Four prototrophic markers were used in this screen: TRP1 and LEU2 for the selection of successful transformation of yeast strains with pAD, pDB plasmids on plates lacking Tryptophan or Leucine, respectively. HIS3 and ADE2 were used for the detection of possible AD-X/DB-Y interactions that reconstitute GAL4 transcription factor in the yeast nucleus and initiate transcription of the reporter gene on media lacking Histidine or Adenine, respectively. Y2H screen (or split GAL4 transcription activator) was done in semi-sterile conditions according to the protocol from Dreze *et al*. (2010). Synthetic complete (SC) selective agar plates that lack the amino acids Leucine and Tryptophan (SC-Leu–Trp) were used to assess mating; interaction plates that further lack Histidine were supplemented with 1 mM 3-amino-1,2,4-triazole (a competitive inhibitor of the HIS3 gene product) (Sc-Leu–Trp–His+1 mM *3AT*) were used to detect the interactions. All DB-X constructs and AD-Y were checked for autoactivation by mating with AD-EV (empty vector) and DB-EV on selection media, respectively.

Agrobacterium-mediated transformation of *N. benthamiana* and BiFC assay

pBIFP2 and pBIFP3 harbouring barley MORCs or putative interactors were transformed into *Agrobacterium tumefaciens* strain GV3101 (pMP90) (Koncz *et al*., 1992, 1994) using a heat-shock method. Positive transformants were selected on YEB plates (for 1 L: 5 g beef extract, 1 g yeast extract, 5 g peptone from soy, 5 g sucrose, 0.5 g $MgCl_2$ and 20 g Agar) complimented with appropriate antibiotics and further confirmed by colony PCR using insert-specific primers (Table S1). Leaves from 4 to 5-week-old *N. benthamiana* plants were used for *Agrobacterium*-mediated transient expression of recombinant proteins. *Agrobacterium* infiltration procedure was performed according to Waadt and Kudla (2008) on the abaxial epidermal leaf layer. The cultures of *Agrobacterium* carrying constructs of interest were set to an optical density (OD_{600}) of 0.5, while culture harbouring the silencing suppressor p19 protein of tomato bushy stunt virus (Chen *et al*., 2011) construct was set to OD_{600} of 0.3. All infiltration combinations for BiFC assay were mixed with p19 before infiltration. Plants were kept at 25 C° for 48 h before visualization under laser scanning confocal microscopy.

Protoplast isolation and transformation

Mesophyll protoplasts were enzymatically released from green leaves of 1–2-week-old barley according to Sheen (1991). After resting on ice for 30 min in WI solution (0.6 M mannitol. 4 mM MES, pH 5.7, 20 mM KCl), the protoplasts were resuspended in MMg solution (4 mM MES, pH 5.7, 0.6 M mannitol, 15 mM $MgC1_2$) to a final of 5×10^5 protoplasts/ml. 200 μL (1×10^5 protoplasts) were used for the PEG-mediated transformation as previously described (Yoo *et al*., 2007). 20–30 μg total plasmid DNA coding for different chimeric N-terminal GFP fusions to the full-length CDS was gently mixed with the protoplasts before slowly adding PEG-Ca^{2+}. Transformation time was set to 13 min. After washing steps as indicated previously (Yoo *et al*., 2007), protoplasts were incubated in modified WI solution (0.6 M mannitol. 4 mM MES, pH 5.7, 4 mM KCl) in the dark at 25 C° for 24 h before visualization using laser scanning confocal microscopy. 10 μg pSAT6-mCherry-VirD2NLS was simultaneously transformed as a nuclear marker.

Confocal laser scanning microscopy

Images were taken using a Leica TCS SP8 confocal laser scanning microscope. GFP::full-length protein samples and BiFC samples were excited using an argon laser at 488 nm and 514 nm,

respectively. YFP and GFP fluorescence emission was detected between 519–548 nm. The nuclear marker (mCherry-VirD2NLS) was excited at 561 nm and fluorescence emission was detected between 573 and 626 nm. Chlorophyll autofluorescence was detected between 679 and 789 nm after excitation using a 633 nm Helium–Neon laser. The pinhole was set to 1 airy unit for both protoplasts and leaf cells. Images for CLSM with nuclear marker were taken in sequential mode, while BiFC images without nuclear marker were acquired in standard mode. YFP-, mCherry fluorescence, and chlorophyll autofluorescence are shown in green, red, and purple, respectively. Images were processed using the Leica LAS X software.

Accession numbers

*Hv*MORC1 [HORVU7Hr1G083280.15], *Hv*MORC2 [HORVU1Hr1G006770.1], *Hv*MORC6a [HORVU3Hr1G046280.3], *Hv*MORC6b [HORVU3Hr1G078330.4], *Hv*MORC7 [HORVU2Hr1G066650.2], *Hv*MORCCW1 [HORVU1Hr1G080470.1], and *Hv*MORCCW2 [HORVU7Hr1G093640.4]; *At*IDN2 [NP_001327083.1], *Hv*IDN2 [BAJ90280.1], *At*SWIC3C [NP_173589.1], *Hv*SWIC3C [BAJ93481.1], *At*DMS3 [NP_566916.1], *Hv*DMS3 [BAJ94830.1], *At*SUVH9 [NP_001031625.1], and *Hv*SUVH9 [BAK07491.1].

Acknowledgements

We thank Martina Claar, Dagmar Biedenkopf, Cornelia Dechert and Eugen Swidtschenko for the excellent technical assistance. This work was funded by the Deutsche Forschungsgemeinschaft (DFG) to KHK (RU5116). M.G. and E.M. were supported by German Academic Exchange Service (DAAD). Open Access funding enabled and organized by Projekt DEAL.

Authorship

M.G., J.S. and K-H.K. wrote the manuscript; KHK, M.G., J.S., N.K., A.K. and J.I. designed the study; M.G., E.M., N.K. and J.I. prepared material for the experiments; M.G., E.M. conducted the experiments; M.G., J.I, J.S. and KHK analysed all data and drafted the figures. All authors commented and reviewed the final manuscript.

Consent for publication

All authors declare consent of publication.

Competing financial interests

The authors declare no competing financial interests.

Data availability statement

All data generated or analysed during this study are included in this published article [and its supplementary information files].

References

Alzohairy, A.M., Yousef, M.A., Edris, S., Kerti, B., Gyulai, G. and Bahieldin, A. (2012) Detection of LTR Retrotransposons Reactivation induced by in vitro Environmental Stresses in Barley (*Hordeum vulgare*) via RT-qPCR. *Life Sci. J.* **9**, 5019–5026.

Azimzadeh, J., Nacry, P., Christodoulidou, A., Drevensek, S., Camilleri, C., Amiour, N., Parcy, F. *et al*. (2008) Arabidopsis TONNEAU1 proteins are essential for preprophase band formation and interact with centrin. *Plant Cell*, **20**, 2146–2159.

Bennetzen, J.L. and Wang, H. (2014) The contributions of transposable elements to the structure, function, and evolution of plant genomes. *Annu. Rev. Plant Biol.* **65**, 505–530.

Blum, M., Chang, H.-Y., Chuguransky, S., Grego, T., Kandasaamy, S., Mitchell, A., Nuka, G. *et al*. (2021) The InterPro protein families and domains database: 20 years on. *Nucleic Acids Res.* **49**(D1), 344–354.

Bordiya, Y., Zheng, Y., Nam, J.C., Bonnard, A.C., Choi, H.W., Lee, B.K., Kim, J. *et al*. (2016) Pathogen infection and MORC proteins affect chromatin accessibility of transposable elements and expression of their proximal genes in Arabidopsis. *Mol. Plant Microbe Interact.* **29**, 674–687.

Brabbs, T.R., He, Z., Hogg, K., Kamenski, A., Li, Y., Paszkiewicz, K.H., Moore, K.A. *et al*. (2013) The stochastic silencing phenotype of Arabidopsis morc6 mutants reveals a role in efficient RNA-directed DNA methylation. *Plant J.* **75**, 836–846.

Braun, P., Tasan, M., Dreze, M., Barrios-Rodiles, M., Lemmens, I., Yu, H., Sahalie, J.M. *et al*. (2009) An experimentally derived confidence score for binary protein-protein interactions. *Nat. Methods*, **6**, 91–97.

Chen, Q., He, J., Phoolcharoen, W. and Mason, H.S. (2011) Geminiviral vectors based on bean yellow dwarf virus for production of vaccine antigens and monoclonal antibodies in plants. *Human Vaccines*, **7**, 331–338.

Citovsky, V., Lee, L.Y., Vyas, S., Glick, E., Chen, M.H., Vainstein, A., Gafni, Y. *et al*. (2006) Subcellular localization of interacting proteins by bimolecular fluorescence complementation *in planta*. *J. Mol. Biol.* **362**, 1120–1131.

Cong, L., Ran, F.A., Cox, D., Lin, S., Barretto, R., Habib, N., Hsu, P.D. *et al*. (2013) Multiplex genome engineering using CRISPR/Cas systems. *Science*, **339**, 819–823.

Dong, W., Vannozzi, A., Chen, F., Hu, Y., Chen, Z. and Zhang, L. (2018) MORC domain definition and evolutionary analysis of the MORC gene family in green plants. *Genome Biol. Evol.* **10**, 1730–1744.

Dreze, M., Monachello, D., Lurin, C., Cusick, M.E., Hill, D.E., Vidal, M. and Braun, P. (2010) High-quality binary interactome mapping. *Methods Enzymol.* **470**, 281–315.

Fernandez-Cornejo, J., Wechsler, S., Livingston, M. & Mitchell, L. (2014). Genetically engineered crops in the United States. USDA-ERS Economic Research Report, (162).

Galindo-González, L., Mhiri, C., Deyholos, M.K. and Grandbastien, M.A. (2017) LTR-retrotransposons in plants: Engines of evolution. *Gene*, **626**, 14–25.

Gasparis, S., Kała, M., Przyborowski, M., Łyżnik, L.A., Orczyk, W. and Nadolska-Orczyk, A. (2018) A simple and efficient CRISPR/Cas9 platform for induction of single and multiple, heritable mutations in barley (*Hordeum vulgare* L.). *Plant Methods*, **14**, 1–14.

Glazebrook, J. (2005) Contrasting mechanisms of defense against biotrophic and necrotrophic pathogens. *Annu. Rev. Phytopathol.* **43**, 205–227.

Govindan, G. and Ramalingam, S. (2016) Programmable site-specific nucleases for targeted genome engineering in higher eukaryotes. *J. Cell. Physiol.* **231**, 2380–2392.

Grandbastien, M.-A., Audeon, C., Bonnivard, E., Casacuberta, J.M., Chalhoub, B., Costa, A.-P., Le, Q.H. *et al*. (2005) Stress activation and genomic impact of Tnt1 retrotransposons in *Solanaceae*. *Cytogenetic Genome Res.* **110**, 229–241.

Harris, C.J., Husmann, D., Liu, W., Kasmi, F.E., Wang, H., Papikian, A., Pastor, W.A. *et al*. (2016) Arabidopsis *At*MORC4 and *At*MORC7 form nuclear bodies and repress a large number of protein-coding genes. *PLoS Genet.* **12**, e1005998.

Holme, I.B., Wendt, T., Gil-Humanes, J., Deleuran, L.C., Starker, C.G., Voytas, D.F. and Brinch-Pedersen, H. (2017) Evaluation of the mature grain phytase candidate *HvPAPhy* a gene in barley (*Hordeum vulgare* L.) using CRISPR/Cas9 and TALENs. *Plant Mol. Biol.* **95**, 111–121.

Huot, B., Yao, J., Montgomery, B.L. and He, S.Y. (2014) Growth–defense tradeoffs in plants: a balancing act to optimize fitness. *Molecular Plant*, **7**, 1267–1287.

Imani, J., Li, L., Schaefer, P. and Kogel, K.H.(2011) STARTS–A stable root transformation system for rapid functional analyses of proteins of the monocot model plant barley. *Plant J.* **67**, 726–735.

International Barley Genome Sequencing Consortium (IBSC). (2012) A physical, genetic and functional sequence assembly of the barley genome. *Nature*, **491**, 711–716.

Iyer, L.M., Abhiman, S. and Aravind, L. (2008) MutL homologs in restriction-modification systems and the origin of eukaryotic MORC ATPases. *Biology Direct*, **3**, 1–9.

Jaganathan, D., Ramasamy, K., Sellamuthu, G., Jayabalan, S. and Venkataraman, G. (2018) CRISPR for crop improvement: an update review. *Frontiers Plant Sci.* **9**, 985.

Jansen, C., Von Wettstein, D., Schäfer, W., Kogel, K.H., Felk, A. and Maier, F.J. (2005) Infection patterns in barley and wheat spikes inoculated with wild-type and trichodiene synthase gene disrupted *Fusarium graminearum*. *Proc. Natl Acad. Sci. USA*, **102**, 16892–16897.

Jarosch, B., Kogel, K.H. and Schaffrath, U. (1999) The ambivalence of the barley Mlo locus: mutations conferring resistance against powdery mildew (*Blumeria graminis f. sp. hordei*) enhance susceptibility to the rice blast fungus *Magnaporthe grisea*. *Mol. Plant Microbe Interact.* **12**, 508–514.

Jing, Y., Sun, H., Yuan, W., Wang, Y., Li, Q., Liu, Y., Li, Y. *et al*. (2016) SUVH2 and SUVH9 couple two essential steps for transcriptional gene silencing in Arabidopsis. *Molecular Plant*, **9**, 1156–1167.

Kang, H.G., Kuhl, J.C., Kachroo, P. and Klessig, D.F. (2008) CRT1, an Arabidopsis ATPase that interacts with diverse resistance proteins and modulates disease resistance to turnip crinkle virus. *Cell Host Microbe.* **3**, 48–57.

Kang, H.G., Oh, C.S., Sato, M., Katagiri, F., Glazebrook, J., Takahashi, H., Kachroo, P. *et al*. (2010) Endosome-associated CRT1 functions early in resistance gene–mediated defense signaling in Arabidopsis and tobacco. *Plant Cell*, **22**, 918–936.

Kang, H.-G., Woo Choi, H., von Einem, S., Manosalva, P., Ehlers, K., Liu, P.-P., Buxa, S.V. *et al*. (2012) CRT1 is a nuclear-translocated MORC endonuclease that participates in multiple levels of plant immunity. *Nat. Commun.* **3**, 1–11.

Kapusi, E., Corcuera-Gómez, M., Melnik, S. and Stoger, E. (2017) Heritable genomic fragment deletions and small indels in the putative ENGase gene induced by CRISPR/Cas9 in barley. *Front. Plant Sci.* **8**, 540.

Karimi, M., Inzé, D. and Depicker, A. (2002) GATEWAY™ vectors for *Agrobacterium*-mediated plant transformation. *Trends Plant Sci.* **7**, 193–195.

Kim, H. and Kim, J.S. (2014) A guide to genome engineering with programmable nucleases. *Nat. Rev. Genet.* **15**, 321–334.

Kis, A., Hamar, É., Tholt, G., Bán, R. and Havelda, Z. (2019) Creating highly efficient resistance against wheat dwarf virus in barley by employing CRISPR/Cas9 system. *Plant Biotechnol. J.* **17**, 1004.

Klessig, D.F., Choi, H.W. and Dempsey, D.M.A. (2018) Systemic acquired resistance and salicylic acid: past, present, and future. *Mol. Plant Microbe Interact.* **31**, 871–888.

Koch, A., Kang, H.G., Steinbrenner, J., Dempsey, D.M.A., Klessig, D.F. and Kogel, K.H. (2017) MORC proteins: novel players in plant and animal health. *Front. Plant Sci.* **8**, 1720.

Koncz, C., Martini, N., Szabados, L., Hrouda, M., Bachmair, A. and Schell, J. (1994) Specialized vectors for gene tagging and expression studies. *Plant Molecul. Biol. Manual*, 53–74.

Koncz, C., Schell, J. and Rédei, G.P. (1992) T-DNA transformation and insertion mutagenesis. *Methods Arabidopsis Res.* 224–273.

Kumar, N., Galli, M., Ordon, J., Stuttmann, J., Kogel, K.H. and Imani, J. (2018) Further analysis of barley MORC 1 using a highly efficient RNA-guided Cas9 gene-editing system. *Plant Biotechnol. J.* **16**, 1892–1903.

Kumar, N., Galli, M., Dempsey, D.M., Imani, J., Moebus, A. and Kogel, K.H. (2021) NPR1 is required for root colonization and the establishment of a mutualistic symbiosis between the beneficial bacterium Rhizobium radiobacter and barley. *Environ. Microbiol.* **23**, 2102–2115.

Langen, G., von Einem, S., Koch, A., Imani, J., Pai, S.B., Manohar, M., Ehlers, K. et al. (2014) The compromised recognition of turnip crinkle virus1 subfamily of microrchidia ATPases regulates disease resistance in barley to biotrophic and necrotrophic pathogens. *Plant physiology* **164**(2), 866–878.

Lawrenson, T., Shorinola, O., Stacey, N., Li, C., Østergaard, L., Patron, N., Uauy, C. *et al*. (2015) Induction of targeted, heritable mutations in barley and Brassica oleracea using RNA-guided Cas9 nuclease. *Genome Biol.* **16**, 1–13.

Lazo, G.R., Stein, P.A. and Ludwig, R.A. (1991) A DNA transformation–competent Arabidopsis genomic library in *Agrobacterium*. *Bio/Technology*, **9**, 963–967.

Lee, J.H., Won, H.J., Hoang Nguyen Tran, P., Lee, S.-M., Kim, H.-Y. and Jung, J.H. (2021) Improving lignocellulosic biofuel production by CRISPR/Cas9-mediated lignin modification in barley. *GCB Bioenergy*, **13**, 742–752.

Li, Y., Liu, D., Zong, Y., Jiang, L., Xi, X., Cao, D., Shen, Y. *et al*. (2020) New D hordein alleles were created in barley using CRISPR/Cas9 genome editing. *Cereal Res. Commun.* **48**, 131–138.

Lin, H.Y., Chen, J.C. and Fang, S.C.(2018) A protoplast transient expression system to enable molecular, cellular, and functional studies in Phalaenopsis orchids. *Front Plant Sci.* **9**, 843.

Liu, Z.W., Shao, C.R., Zhang, C.J., Zhou, J.X., Zhang, S.W., Li, L., Chen, S. *et al*. (2014) The SET domain proteins SUVH2 and SUVH9 are required for Pol V occupancy at RNA-directed DNA methylation loci. *PLoS Genet.* **10**, e1003948.

Liu, Z.W., Zhou, J.X., Huang, H.W., Li, Y.Q., Shao, C.R., Li, L., Cai, T. *et al*. (2016) Two components of the RNA-directed DNA methylation pathway associate with MORC6 and silence loci targeted by MORC6 in Arabidopsis. *PLoS Genet.* **12**, e1006026.

Lorković, Z.J., Naumann, U., Matzke, A.J. and Matzke, M. (2012) Involvement of a GHKL ATPase in RNA-directed DNA methylation in *Arabidopsis thaliana*. *Curr. Biol.* **22**, 933–938.

Mali, P., Yang, L., Esvelt, K.M., Aach, J., Guell, M., DiCarlo, J.E., Norville, J.E. *et al*. (2013) RNA-guided human genome engineering via Cas9. *Science*, **339**, 823–826.

Manohar, M., Choi, H.W., Manosalva, P., Austin, C.A., Peters, J.E. and Klessig, D.F. (2017) Plant and human MORC proteins have DNA-modifying activities similar to type II topoisomerases, but require one or more additional factors for full activity. *Mol. Plant Microbe Interact.* **30**, 87–100.

Manosalva, P., Manohar, M., Kogel, K.H., Kang, H.G. and Klessig, D.F. (2015) The GHKL ATPase MORC1 modulates species-specific plant immunity in Solanaceae. *Mol. Plant Microbe Interact.* **28**, 927–942.

Moissiard, G., Bischof, S., Husmann, D., Pastor, W.A., Hale, C.J., Yen, L., Stroud, H. *et al*. (2014) Transcriptional gene silencing by Arabidopsis microrchidia homologues involves the formation of heteromers. *Proc. Natl Acad. Sci. USA*, **111**, 7474–7479.

Moissiard, G., Cokus, S.J., Cary, J., Feng, S., Billi, A.C., Stroud, H., Husmann, D. *et al*. (2012) MORC family ATPases required for heterochromatin condensation and gene silencing. *Science*, **336**, 1448–1451.

Pieterse, C.M., Van der Does, D., Zamioudis, C., Leon-Reyes, A. and Van Wees, S.C. (2012) Hormonal modulation of plant immunity. *Annu. Rev. Cell Dev. Biol.* **28**, 489–521.

Salazar, M., González, E., Casaretto, J.A., Casacuberta, J.M. and Ruiz-Lara, S. (2007) The promoter of the TLC1. 1 retrotransposon from *Solanum chilense* is activated by multiple stress-related signaling molecules. *Plant Cell Rep.* **26**, 1861–1868.

Sheen, J. (1991) Molecular mechanisms underlying the differential expression of maize pyruvate, orthophosphate dikinase genes. *Plant Cell*, **3**, 225–245.

Waadt, R. and Kudla, J. (2008) In planta visualization of protein interactions using bimolecular fluorescence complementation (BiFC). *Cold Spring Harbor Protocols*, **2008**, 4995.

Xu, G., Yuan, M., Ai, C., Liu, L., Zhuang, E., Karapetyan, S., Wang, S. *et al*. (2017) uORF-mediated translation allows engineered plant disease resistance without fitness costs. *Nature*, **545**, 491–494.

Xue, Y., Zhong, Z., Harris, C.J., Gallego-Bartolomé, J., Wang, M., Picard, C., Cao, X., Hua, S., Kwok, I., Feng, S. and Jami-Alahmadi, Y. (2021) Arabidopsis MORC proteins function in the efficient establishment of RNA directed DNA methylation. *Nature communications*, **12**, 1–13.

Yi, Z., Sanjeev, M. and Singh, G. (2020) The branched nature of the nonsense-mediated mRNA decay pathway. *Trends Genet.* **37**, 143–159.

Yoo, S.D., Cho, Y.H. and Sheen, J. (2007) Arabidopsis mesophyll protoplasts: a versatile cell system for transient gene expression analysis. *Nat. Protoc.* **2**, 1565–1572.

Yu, A., Lepère, G., Jay, F., Wang, J., Bapaume, L., Wang, Y., Abraham, A.L. *et al*. (2013) Dynamics and biological relevance of DNA demethylation in Arabidopsis antibacterial defense. *Proc. Natl Acad. Sci. USA*, **110**, 2389–2394.

Zeng, Z., Han, N., Liu, C., Buerte, B., Zhou, C., Chen, J., Wang, M. *et al*. (2020) Functional dissection of HGGT and HPT in barley vitamin E biosynthesis via CRISPR/Cas9-enabled genome editing. *Ann. Bot.* **126**, 929–942.

Zhu, H., Li, C. and Gao, C. (2020) Applications of CRISPR–Cas in agriculture and plant biotechnology. *Nat. Rev. Mol. Cell Biol.* **21**, 661–677.

Supporting information

Additional supporting information may be found online in the Supporting Information section at the end of the article.

Figure S1 *HvMorc6*-sgRNA target location and construct used to generate *hvmorc6a* barley mutants. (a) Schematic representation of the T-DNA region containing all components for *Agrobacterium*-mediated, *Sp*Cas9-based *HvMORC6a* gene editing. *pCMV35s*, *Cauliflower Mosaic Virus* 35S promoter, *hpt*, *hygromycin phosphotransferase gene*; *t35s*, *CaMV* 35S terminator; *pHvU3*, barley *U3* promoter; target *morc6a* sequence; *sgRNA*, synthetic single-guide RNA; pZmUbi, ubiquitin promoter of *Zea mays*; *SpCas9*, *S. pyogenes* Cas9; *LB*, *RB*, left and right border sequences of the T-DNA. (b) Target area of *hvmorc1*-sgRNA and *hvmorc6a*-sgRNA (20 nt, underlined) with PAM sequence (grey highlighted) in *Hv*MORC1 and *Hv*MORC6a protein architecture, respectively; hallmark domains (HATPase_C, S5, and CC) are highlighted in bounding boxes; thunder indicates precise location of *Sp*Cas9 cutting site. Protein domains were drawn after analysis of the protein sequence via the InterPro protein families and domains database (https://www.ebi.ac.uk/interpro/; Blum *et al*., 2021). Note both protein domain structures have been drawn to scale. (c) Target area of *hvmorc6a*-sgRNA in *HvMORC6a* cDNA sequence. (d) Alignment of potential target sites of the *hvmorc6a*-sgRNA in other *HvMORC* paralogs; similar nucleotides to the sgRNA are displayed in red.

Figure S2 CRISPR/*Sp*Cas9 efficiency and cleavage sites in *hvmorc6a* barley mutant lines. (a) Schematic summary of the transformation efficiency in *Sp*Cas9-induced *hvmorc6a* mutants. (b) Homozygous mutations in T0 *hvmorc6a* plants, determined after sequencing using specific primers (Table S1). The PAM (NGG) sequence is highlighted in grey, the 20 bp long target region is underlined, and point mutations are marked in bold. (c) All bi-allelic homozygous mutation patterns found in independent plants. (d) Example of a heterozygous mutant, with the characteristic multiple spikes in the chromatogram.

Figure S3 *Sp*Cas9-induced frame-shift mutations in *HvMORC1* and *HvMORC6a*. (a) Homozygous mutated lines used in this study: *hvmorc1* (Δ*hvmorc1*-L3), *hvmorc6a* (Δ*hvmorc6a*-L9 and L16), and *hvmorc1/6a* (Δ*hvmorc1/6a*-L4 and L5) T3 homozygous mutants. (b) CRISPR/*Sp*Cas9 system inserts STOP codons in *HvMORC1* and *HvMORC6a* open reading frames (in red), leading to the premature termination of the protein. Frame-shift mutations are visualized via the online tool (http://web.expasy.org/translate/).

Figure S4 YFP signals of homo-/heteromerization of different *Hv*MORCs. *Hv*MORCs combinations were detected in lower epidermal cells of tobacco after 48 h (left panel). pBiFP2-*Hv*MORCs and pBiFP3-*Hv*MORCs were N-terminally fused to the N- and C- terminal parts of YFP, respectively. The different combinations show similar interaction results. ROI is a magnification of the bordered region in the overlay column. Scale bar: 20 μm. YFP: yellow fluorescence protein, Chl: chlorophyll autofluorescence, ROI: regions of interest (magnification of the bordered region).

Figure S5 GFP::*Hv*DMS3 localization and YFP signals of homo-/heteromerization of different *Hv*MORCs with orthologs of the RdDM pathway. (a) The interaction between barley MORCs and SWI3C, and IDN2 was detected in both combination directions of the two BiFC vectors in lower epidermal cells of tobacco. Scale bar, 20 μm. (b) Localization of *Hv*DMS3 in barley WT and *hvmorc6a* protoplasts, and interaction between barley MORCs and DMS3 (no signal detected in both directions). Scale bar, 20 μm. YFP: yellow fluorescence protein, Chl: chlorophyll autofluorescence, ROI: regions of interest (magnification of the bordered region).

Table S1 Oligonucleotide primers used in this study.

Table S2 Barley orthologs of the potential Arabidopsis RdDM interactors.